soil systems

MDPI

Article

Interaction of Natural Heulandite–Clinoptilolite Zeolite with Real Acid Mine Drainage: Metal Removal, pH Evolution, and Mineralogical–Microchemical Transformations

Gabriela Alvarado-Macías [1], Dora P. Nava-Gómez [1], Jonatan Andrade-Martínez [1], Erik Espinosa-Serrano [1,*], Iván A. Reyes [2,3] and Gilberto Rosales-Marín [1,2,*]

[1] Unidad Académica Multidisciplinaria Región Altiplano, Universidad Autónoma de San Luis Potosí, Carretera a Cedral km 5+600, Matehuala 78700, Mexico; gabriela.alvarado@uaslp.mx (G.A.-M.); dora.nava@uaslp.mx (D.P.N.-G.); jonatan.andrade@uaslp.mx (J.A.-M.)
[2] Instituto de Metalurgia, Facultad de Ingeniería, Universidad Autónoma de San Luis Potosí, Av. Sierra Leona 550, Lomas 2ª Sección, San Luis Potosí 78210, Mexico; alejandro.reyes@uaslp.mx
[3] Secretaría de Ciencias, Humanidades, Tecnología e Innovación (SECIHTI), Insurgentes Sur 1582, Mexico City 03940, Mexico
* Correspondence: erik.espinosa@uaslp.mx (E.E.-S.); gilberto.rosales@uaslp.mx (G.R.-M.)

Abstract

Acid mine drainage (AMD) is characterized by low pH and elevated dissolved Cu and Pb concentrations, requiring effective treatment while minimizing secondary waste generation. This study investigates the interaction of natural heulandite–clinoptilolite zeolite with real AMD, focusing on metal removal, solution chemistry, and post-treatment mineralogical and microchemical transformations. Batch experiments used 3.5, 7.5, and 15.0 g of zeolite per 100 mL of AMD, with Cu and Pb removal monitored for 360 min. Initial AMD pH was 3.6 and increased rapidly, stabilizing at approximately 4.3, 5.2, and 6.2 with increasing zeolite dosage. Cu and Pb were rapidly removed, with near-complete removal of Cu and Pb at the highest dosage within 45 min. Kinetic analysis showed that the pseudo-second-order model generally provided the best empirical fit, while Weber–Morris analysis indicated that intraparticle diffusion was not the sole rate-controlling mechanism. X-ray diffraction showed that the principal heulandite–clinoptilolite crystalline phases remained identifiable after treatment, although reflections compatible with Cu-exchanged clinoptilolite and Ca–SO_4-bearing phases were also detected. SEM-EDS revealed localized Cu-rich regions containing up to 52.09 wt.% Cu and localized Fe-rich domains in the post-treatment material. Although Pb was efficiently removed from solution, it was not detected in the analyzed post-treatment crystalline or localized solid phases. Overall, natural heulandite–clinoptilolite substantially modified AMD chemistry and removed dissolved Cu and Pb while the principal zeolitic crystalline phases remained identifiable after treatment and localized chemical transformations were detected.

Keywords: acid mine drainage; natural zeolite; metal removal; sorption; mineralogical transformations

Check for updates

Academic Editor: René H. Lara

Received: 24 August 2026
Revised: 24 September 2026
Accepted: 25 September 2026
Published: 14 October 2026

Copyright: © 2026 by the authors. Licensee MDPI, Basel, Switzerland. This article is an open access article distributed under the terms and conditions of the Creative Commons Attribution (CC BY) license.

1. Introduction

Acid mine drainage (AMD) is one of the most significant environmental challenges associated with mining activities. It is generated through the oxidation of sulfide minerals, producing acidic effluents characterized by elevated concentrations of dissolved metals

and sulfate ions. The discharge of untreated AMD can severely affect aquatic ecosystems, soil quality, and water resources due to its persistence and toxicity [1,2].

Among the various treatment technologies available for AMD remediation, sorption has attracted considerable attention because of its operational simplicity, cost-effectiveness, and potential for selective removal of dissolved metal ions. Natural zeolites, particularly clinoptilolite-rich materials, have been extensively investigated as adsorbents owing to their high cation exchange capacity, porous structure, chemical stability, and widespread availability [3]. Previous studies have demonstrated the effectiveness of natural zeolites for the removal of metal ions such as Fe, Cu, Zn, Mn, Cd, and Pb from mine-impacted waters through a combination of ion exchange and surface sorption mechanisms [4,5].

Despite these promising results, most previous investigations have focused on synthetic solutions or simplified metal systems, whereas the behavior of natural zeolites in treating real AMD remains comparatively less understood. Real AMD contains complex mixtures of competing cations, sulfate species, and variable acidity that may modify both metal-removal performance and the interaction between the aqueous phase and the zeolitic structure. Previous studies using natural zeolites have demonstrated effective removal of dissolved metals from mine waters and AMD, but the extent to which treatment modifies the mineralogical and microchemical characteristics of the zeolite remains insufficiently resolved [4–7].

In addition, previous studies have investigated natural zeolites for metal removal from mine-impacted waters under both batch and dynamic conditions. Batch studies have evaluated the effects of contact time, zeolite dosage, pH, and competing ions on metal removal [5], whereas dynamic column experiments have examined the performance of natural zeolite using real AMD under continuous-flow conditions [7]. More recently, batch experiments with natural clinoptilolite and real AMD have further highlighted the importance of zeolite dosage and solution chemistry in controlling treatment performance [8]. However, the temporal relationship between solution pH evolution, metal removal, and changes in the mineralogical and microchemical characteristics of the zeolitic material during contact with real AMD remains insufficiently resolved. This aspect is particularly relevant because the increase in pH accompanying zeolite–AMD interaction may modify the chemical environment and influence the processes responsible for dissolved-metal removal. Therefore, the main objective of this study was to elucidate how the interaction between natural heulandite–clinoptilolite and real AMD affects both aqueous-phase metal removal and the chemical and mineralogical characteristics of the zeolitic material. Specifically, the study evaluates the coupled evolution of solution pH, Cu and Pb removal kinetics, and post-treatment mineralogical and localized microchemical changes using aqueous-phase analysis, kinetic modeling, XRD, and SEM-EDS.

2. Materials and Methods

2.1. Natural Zeolite and AMD Characterization

Natural zeolite was used as the sorbent for real acid mine drainage (AMD) treatment. Its mineralogical composition and morphology were characterized by X-ray diffraction (XRD) and scanning electron microscopy coupled with energy-dispersive X-ray spectroscopy (SEM-EDS), respectively. Prior to the batch experiments, the zeolite was crushed and dry-ground, and its particle-size distribution was determined by mechanical sieving using Tyler sieves arranged according to the $\sqrt{2}$ series of sieve openings. The natural zeolite sample was obtained directly from a zeolite processing plant, where the material was being treated, and was kindly provided for research purposes. The sample was crushed and dry-ground, and the resulting material was sieved to obtain an average particle size of 124 μm. No chemical pretreatment was applied before the experiments.

Real AMD was collected directly from mine tailings in the Real de Catorce region, San Luis Potosí, Mexico. The collected AMD was stored in an HDPE container at ambient temperature and used within a few days of collection. The leachate had a pH of 3.6. Dissolved elemental concentrations were determined by inductively coupled plasma optical emission spectrometry (ICP-OES) using a Thermo Scientific iCAP 7000 Series instrument. Sulfur was measured as total dissolved sulfur and reported as S. An estimated sulfate concentration of approximately 16,900 mg L^{-1} was calculated assuming that dissolved sulfur occurred predominantly as sulfate. This value represents an estimate rather than a direct sulfate measurement. Sulfate was not directly quantified in the present study; therefore, the estimated sulfate concentration is used only to indicate the high sulfur/sulfate character of the AMD and is not considered a measured sulfate concentration, a complete anion inventory, or an ionic balance [1,2].

2.2. Batch Sorption Experiments

Batch experiments were performed by contacting 3.5, 7.5, and 15.0 g of zeolite with 100 mL of AMD in 200-mL high-density polyethylene (HDPE) bottles. Three independent reactors were prepared for each combination of zeolite dosage and contact time (n = 3). Accordingly, the kinetic experimental matrix comprised three zeolite dosages, eight contact times, and three independent reactors per condition, corresponding to 72 independent batch reactors. This design allowed the effects of zeolite dosage and contact time to be evaluated independently while providing replicate measurements for each experimental condition. The suspensions were agitated at 150 rpm at 22 ± 2 °C. Independent reactors were used for each contact time to avoid changes in zeolite mass, solution volume, solid-to-liquid ratio, and dissolved-ion inventory associated with repeated sampling from a single reactor. At each predetermined contact time, the corresponding reactor was removed from agitation and the suspension was filtered using qualitative filter paper (Fisherbrand QL100). The filtrates were analyzed by ICP-OES. The experimental approach was based on previously reported batch studies of natural zeolite for the removal of dissolved metals from AMD [4,5].

2.3. Sorption Kinetics and Dosage Effect

Sorption kinetics were evaluated at contact times of 5, 15, 30, 45, 60, 120, 240 and 360 min using 3.5, 7.5 and 15 g of zeolite per 100 mL of AMD. Sorption capacity and removal efficiency were calculated as

$$q_t = (C_0 - C_t)\frac{V}{m} \quad (1)$$

$$R(\%) = \frac{(C_0 - C_t)}{C_0} \cdot 100 \quad (2)$$

where C_0 and C_t are the initial and residual dissolved-metal concentrations (mg L^{-1}), respectively; V is the solution volume (L); and m is the mass of zeolite (g).

The analytical limits of quantification (LOQ) were 0.0716 mg L^{-1} for Cu and 0.0108 mg L^{-1} for Pb. Residual Cu and Pb concentrations reported as 0.00 mg L^{-1} by the analytical procedure were interpreted as concentrations below the corresponding LOQ rather than as true zero concentrations. For the kinetic calculations, observations reported as 0.00 mg L^{-1} in the original analytical dataset were retained as 0.00 mg L^{-1} for the calculation of q_t and subsequent model fitting. Thus, these values were treated as below-LOQ observations analytically, rather than as evidence of complete absence of the corresponding metal. The kinetic data were fitted using nonlinear pseudo-first-order (PFO) and pseudo-second-order (PSO) models. Model performance was evaluated using the coefficient of

determination (R^2) and the sum of squared errors (SSE). SSE was calculated as the sum of the squared differences between the experimental and model-predicted sorption capacities:

$$SSE = \sum_{i=1}^{n} (q_{t,i,\text{exp}} - q_{t,i,\text{model}})^2 \quad (3)$$

The coefficient of determination was calculated as

$$R^2 = 1 - \frac{SSE}{SST} \quad (4)$$

$$SST = \sum_{i=1}^{n} (q_{t,i,\text{exp}} - \bar{q}_{t,\text{exp}})^2, \quad (5)$$

where $q_{t,i}^{exp}$ and $q_{t,i}^{model}$ are the experimental and model-predicted sorption capacities at time i, respectively, and $q_t^{\bar{exp}}$ is the mean experimental sorption capacity. Higher R^2 values and lower SSE values indicate closer agreement between the experimental and model-predicted values. The model showing the combination of higher R^2 and lower SSE was considered to provide the closer empirical fit to the experimental data.

$$q_t = q_e(1 - e^{(-k1t)}) \quad (6)$$

$$q_t = \frac{k_2 q_e^{2t}}{(1 + k_2 q_e t)} \quad (7)$$

The PFO formulation is derived from the Lagergren approach [9], while the PSO model follows the formulation proposed by Ho and McKay [10].

The operational equilibrium was defined as the shortest time at which further increases in contact time produced no appreciable improvement in removal.

To further investigate the rate-controlling processes during sorption, the Weber–Morris [11] intraparticle diffusion model was applied. This model describes sorbate uptake as a function of the square root of contact time and is expressed as:

$$q_t = k_{id} t^{1/2} + C \quad (8)$$

where k_{id} is the intraparticle diffusion rate constant (mg g^{-1} $min^{-1/2}$), t is the contact time (min), and C is the intercept associated with the boundary-layer effect (mg g^{-1}). The model was originally proposed by Weber and Morris [11] and is commonly used to assess the contribution of intraparticle diffusion to the overall sorption process.

A plot of q_t versus $t^{1/2}$ was used to evaluate the linearity of the sorption process. If the plot passes through the origin, intraparticle diffusion can be considered the predominant rate-controlling step; conversely, a non-zero intercept indicates that other processes, such as boundary-layer diffusion, also contribute to sorption. Therefore, the Weber–Morris model was used as a complementary analysis to the PFO and PSO models rather than as a standalone mechanistic criterion.

The effect of zeolite dosage was subsequently evaluated at the operational equilibrium using 3.5, 7.5, and 15.0 g of zeolite per 100 mL of AMD. Equilibrium sorption capacity was calculated as

$$q_e = \frac{(C_o - C_e)V}{m} \quad (9)$$

where C_e is the residual concentration at the operational equilibrium (mg L^{-1}). The effect of zeolite dosage was evaluated in terms of residual Cu or Pb concentration, removal efficiency, and sorption capacity to characterize the performance of natural zeolite in the multicomponent AMD matrix.

2.4. Monitoring of pH During Zeolite–AMD Interaction

The pH evolution during zeolite–AMD interaction was monitored at 5, 15, 30, 45, 60, 120, 240, and 360 min for zeolite dosages of 3.5, 7.5, and 15.0 g per 100 mL of AMD. Measurements were performed directly in the suspension using a potentiometer (pH Meter Model 700), previously calibrated using standard buffer solutions at pH 4 and pH 10. At each sampling time, the suspension was temporarily removed from agitation for pH measurement without withdrawing an aliquot, thereby maintaining the original solid-to-liquid ratio throughout the experiment. After measurement, the electrode was rinsed and dried before continuing the treatment.

2.5. Post-Treatment Characterization

After treatment, the zeolite recovered from the final experimental condition (15.0 g of zeolite per 100 mL of AMD and 360 min of contact time) was dried at 30 °C for 72 h prior to characterization. The dried material was subsequently characterized by X-ray diffraction (XRD) and scanning electron microscopy coupled with energy-dispersive X-ray spectroscopy (SEM-EDS). XRD analyses were performed using a Bruker D8 Advance diffractometer with Cu Kα radiation (λ = 1.5406 Å). XRD patterns were collected over a 2θ range of approximately 5–90° and compared with reference patterns from the Powder Diffraction File (PDF) database for phase identification. For SEM-EDS analysis, the dried material was mounted on a specimen stub and carbon-coated prior to analysis. SEM imaging was performed at micrometer-scale resolution, and EDS spectra were collected for localized elemental characterization of selected regions of the zeolite surface. The treated and untreated materials were compared to assess changes in crystalline phases, morphology, surface texture, and localized elemental composition following exposure to AMD.

2.6. Mechanistic Interpretation

The interaction mechanism was interpreted by integrating the AMD chemical composition with the kinetic, equilibrium, XRD, and SEM-EDS results, with emphasis on cation exchange, surface sorption, and possible secondary-phase formation or metal accumulation, as reported for natural zeolite–metal systems [3,4].

3. Results and Discussion

3.1. Initial Characterization of Natural Heulandite–Clinoptilolite and Real AMD

The X-ray diffraction (XRD) pattern of the natural zeolite (Figure 1) indicates that the material is predominantly composed of Ca-bearing heulandite and clinoptilolite. These zeolitic phases contain negatively charged aluminosilicate frameworks compensated by exchangeable cations, mainly Ca^{2+}, Na^{+}, and K^{+}, providing sites for cation exchange and Cu and Pb uptake [3,4]. The mineralogical composition is consistent with previous studies reporting natural clinoptilolite and related zeolitic materials as effective sorbents for dissolved metals in mine waters and AMD [5,7].

The AMD sample collected from an active sulfide tailing storage facility exhibited a pH of 3.6. The leachate contained 197.4 mg L^{-1} Cu, 2.05 mg L^{-1} Pb, 5639.6 mg L^{-1} S, 11,360.8 mg L^{-1} Na, and 174.9 mg L^{-1} K (Table 1), while Al, Zn, Mn, Cd, Cr, Co, Ni, and As were below the analytical limit of quantification. Assuming that dissolved sulfur occurred predominantly as sulfate, its concentration was estimated at approximately 16.9 g L^{-1} SO_4^{2-}. The drainage originated from a sulfide tailing facility associated with a previous hydrometallurgical Cu recovery process using sulfuric acid, sodium thiosulfate, potassium hydroxide, nitrite, and copper-containing reagents. Thus, its composition reflects both sulfide-tailing weathering and the previous processing history. In particular, sodium

thiosulfate and potassium hydroxide provide plausible sources for the elevated Na and K concentrations, respectively, although their contributions cannot be quantified because historical reagent consumption was unavailable.

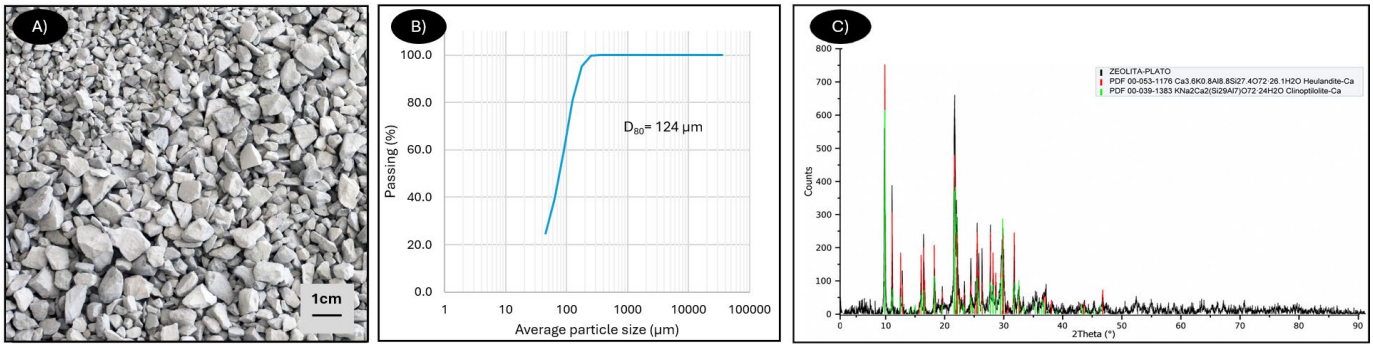


Figure 1. Characterization of the natural heulandite–clinoptilolite zeolite used in this study: (**A**) representative macroscopic photograph of the raw zeolitic material with scale reference, (**B**) particle-size distribution determined by mechanical sieving, and (**C**) XRD pattern of the untreated zeolite with reference patterns for heulandite-Ca and clinoptilolite-Ca.

Table 1. AMD Chemical composition from an active sulfide tailing.

Element	mg L^{-1}	L.O.C. (mg L^{-1})
Cu	197.4	0.0716
Pb	2.05	0.0108
Na	11,360.8	0.8386
K	174.9	0.4852
Ca	1.67	0.0607
Mg	0.22	0.1015
Fe	0.19	0.1656
Al	<LOQ	0.6078
Zn	<LOQ	0.0877
Mn	<LOQ	0.1015
Cd	<LOQ	0.0894
Cr	<LOQ	0.3195
Co	<LOQ	0.0765
Ni	<LOQ	0.0912
As	<LOQ	0.1052
pH		3.6
Estimated SO_4^{2-} (mg L^{-1})		16,900

The combination of low pH and a high sulfate concentration is characteristic of AMD generated through sulfide-mineral oxidation [1,2]. The relatively high Cu concentration identifies Cu as the main target metal for the subsequent treatment experiments, while Pb occurs at a substantially lower concentration. The elevated Na^+ and K^+ concentrations may also contribute to competition for zeolitic exchange sites in the multicomponent AMD matrix [5].

Overall, the initial characterization confirms a Ca-bearing heulandite–clinoptilolite zeolite and an acidic, sulfate-rich AMD containing measurable Cu and Pb. These characteristics provide the basis for evaluating the effects of contact time, zeolite dosage, sorption kinetics, and equilibrium behavior. The combination of AMD acidity, dissolved-metal composition, and zeolite dosage provides the chemical framework for evaluating the treatment

response. Recent work using clinoptilolite with natural AMD has similarly highlighted the influence of zeolite dosage and solution chemistry on metal-removal performance [8].

3.2. Evolution of Solution pH During Treatment

The initial AMD exhibited a pH of 3.6. Contact with the natural heulandite–clinoptilolite zeolite produced a rapid and dose-dependent increase in pH, particularly during the first 30–60 min of treatment (Figure 2). At the end of the experiments, the pH increased to 4.30, 5.20, and 6.20 for zeolite dosages of 3.5, 7.5, and 15.0 g per 100 mL of AMD, respectively. Thus, the corresponding changes in pH were 0.70, 1.60, and 2.60 units, demonstrating that increasing the zeolite dosage substantially modified the acid–base conditions of the AMD.

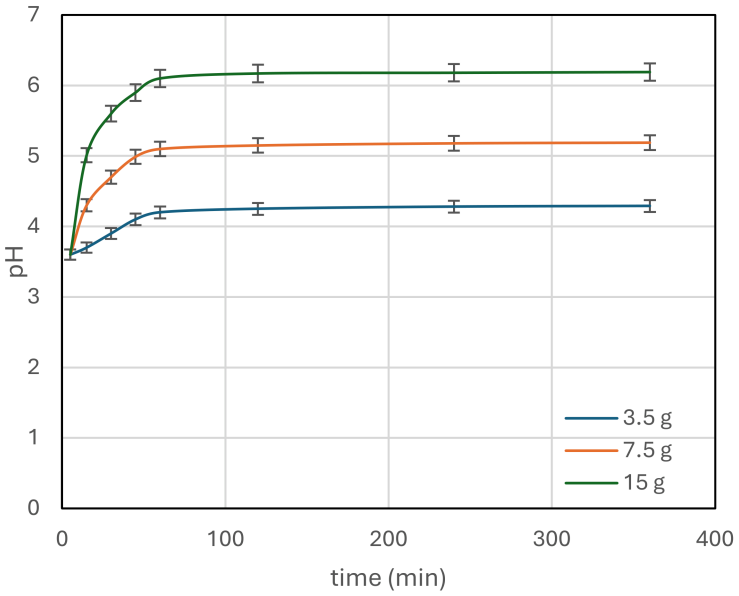


Figure 2. Experimental evolution of solution pH during contact of real acid mine drainage with natural heulandite–clinoptilolite at zeolite dosages of 3.5, 7.5, and 15.0 g per 100 mL of AMD.

The pH profiles shown in Figure 2 also exhibited a rapid initial stage followed by stabilization. For all dosages, most of the pH increase occurred within the first 30–60 min, after which only minor changes were observed up to 360 min. This behavior indicates that the interaction between the zeolite and the acidic AMD was particularly intense during the initial contact period. The dose-dependent increase in pH is consistent with the cation-exchange and acid–base properties of natural zeolites, although the individual contribution of these processes cannot be distinguished from the present data. This rapid increase followed by stabilization is consistent with the behavior reported for clinoptilolite-based treatment of natural AMD, where increasing zeolite dosage was associated with an increase in solution pH [8]. The magnitude of the pH response observed in the present study is nevertheless specific to the chemical composition of the AMD and the zeolite-to-liquid ratio used here.

The temporal evolution of pH is relevant to the metal-removal results discussed below because the most pronounced changes in pH occurred during the same initial period in which Cu and Pb were rapidly removed from the aqueous phase. This temporal association suggests that changes in the chemical conditions of the AMD accompanied metal uptake, although the present data do not establish a direct causal relationship between pH increase and Cu and Pb removal.

3.3. Cu and Pb Removal Kinetics

3.3.1. Metal Sorption of Cu and Pb

Figure 3 shows the removal kinetics of Cu and Pb from real AMD using 3.5, 7.5, and 15 g of natural zeolite. Both Cu and Pb exhibited rapid removal, although their kinetic profiles differed. Cu showed a particularly fast response at all zeolite dosages. At 3.5 g, Cu removal reached 98.63% within 60 min, while the residual Cu concentration was below the analytical LOQ after 240 min. Increasing the dosage to 7.5 g resulted in 96.30% removal within 30 min, while the residual Cu concentration was below the analytical LOQ after 120 min, whereas 15 g achieved 97.56% removal within the first 5 min, with the residual Cu concentration falling below the analytical LOQ after 45 min. Thus, increasing the zeolite dosage primarily accelerated Cu removal.

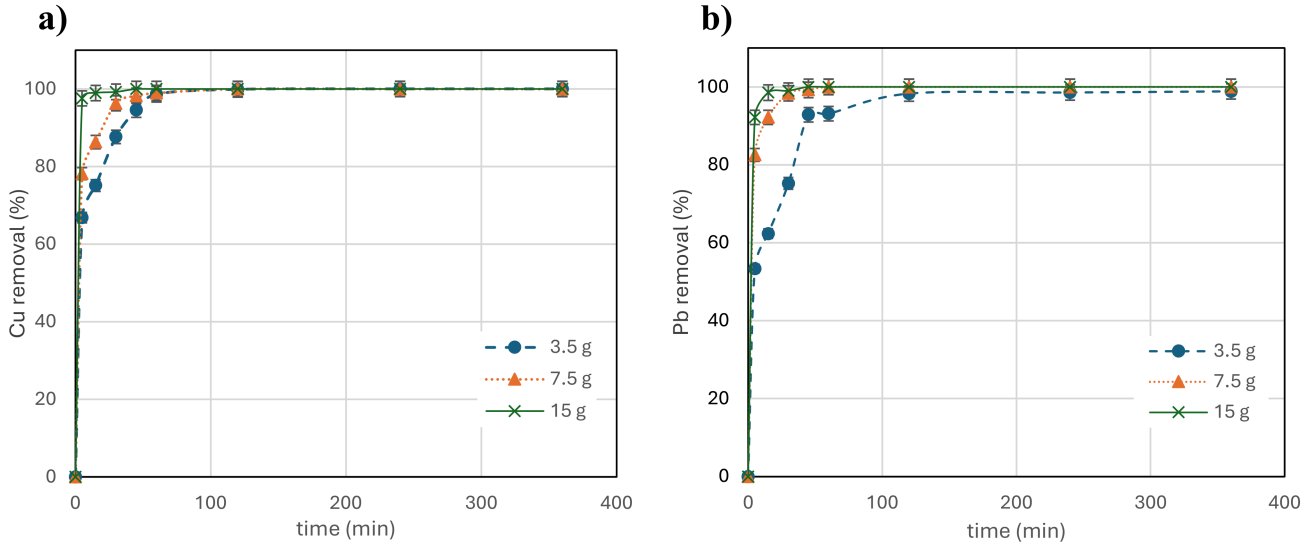


Figure 3. Removal kinetics of dissolved metals from real acid mine drainage using natural zeolite at different dosages: (**a**) Cu and (**b**) Pb.

Pb showed a comparatively slower removal profile, particularly at 3.5 g. Under this condition, Pb removal increased from 53.36% at 5 min to 92.86% at 45 min and 98.86% at 360 min. Increasing the dosage accelerated the process, with 7.5 g achieving 98.36% removal within 30 min, while the residual Pb concentration fell below the analytical LOQ after 60 min. At 15 g, Pb removal reached 92.20% within 5 min, with the residual Pb concentration falling below the analytical LOQ after 45 min. Therefore, increasing the zeolite dosage substantially reduced the contact time required to achieve near-complete removal of both metals.

The different Cu and Pb kinetic profiles are particularly relevant because the experiments were conducted using real AMD containing multiple dissolved species. The initial Cu concentration (197.4 mg L^{-1}) was approximately 96 times higher than that of Pb (2.05 mg L^{-1}), resulting in substantially different concentration gradients and mass-transfer driving forces. In addition, the solution pH increased rapidly during the initial contact period, with the magnitude of the increase depending strongly on zeolite dosage. Thus, the rapid removal of both metals occurred concurrently with substantial changes in the chemical conditions of the AMD. This temporal association indicates that metal uptake was accompanied by changes in solution chemistry, although the present data do not establish a direct causal relationship between pH evolution and Cu and Pb removal. Metal speciation, competition among dissolved ions, ion exchange, surface interactions, precipitation, and mass-transfer processes may contribute simultaneously to the observed removal kinetics, as expected for multicomponent mine-water systems treated with natural zeolites [4,5].

The corresponding sorption capacities are presented in Figure 4. For Cu, q_t increased rapidly during the initial stage and subsequently approached a plateau. The highest experimental capacity was obtained with 3.5 g, reaching 5.64 mg g^{-1}, compared with 2.63 and 1.32 mg g^{-1} for 7.5 and 15 g, respectively. Thus, although increasing the zeolite dosage accelerated Cu removal, it decreased the Cu loading per unit mass of zeolite. This behavior is expected in batch systems with a fixed initial metal inventory, where increasing the adsorbent mass increases the number of available sites relative to the finite amount of dissolved metal.

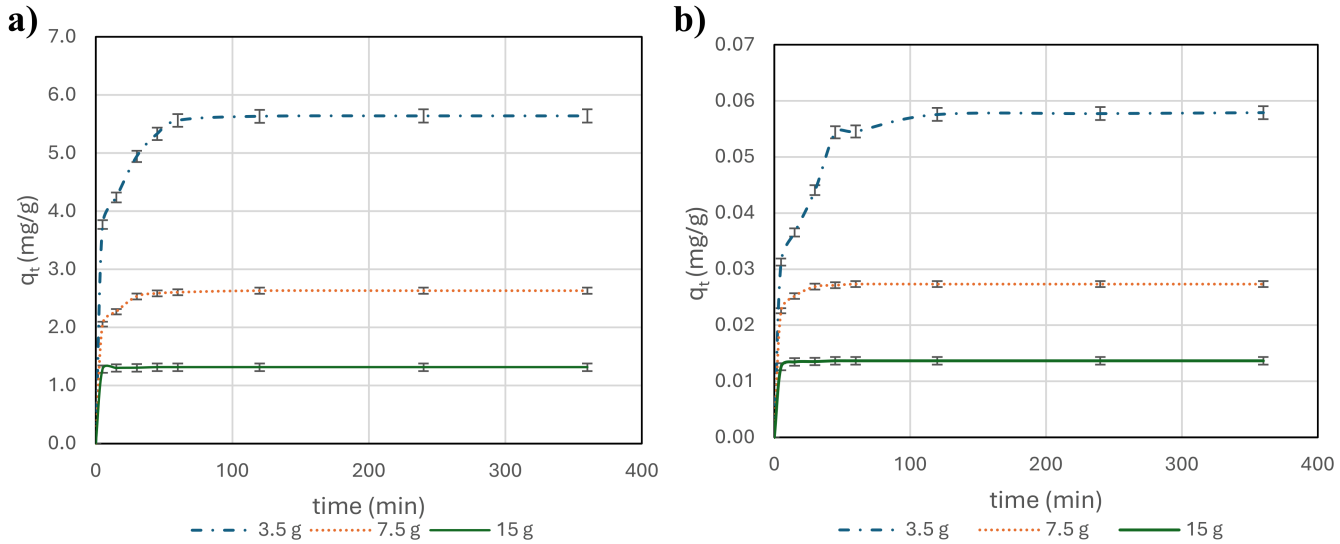


Figure 4. Sorption capacity (q_t) of natural zeolite for dissolved metals in real acid mine drainage as a function of contact time: (**A**) Cu and (**B**) Pb.

For Pb, values were considerably lower, reaching approximately 0.059 mg g^{-1} with 3.5 g, 0.027 mg g^{-1} with 7.5 g, and 0.0137 mg g^{-1} with 15 g. This lower loading is consistent with the substantially lower initial Pb concentration in the AMD. Overall, the results reveal a clear distinction between removal efficiency and sorption capacity: increasing the zeolite dosage enhanced the removal rate and shortened the contact time required for near-complete Cu and Pb removal, whereas lower dosages favored higher metal loading per unit mass.

3.3.2. PFO and PSO Kinetic Modeling

Figure 5 and Table 2 present the fitting of the pseudo-first-order (PFO) and pseudo-second-order (PSO) kinetic models to the experimental Cu and Pb removal data. For Cu, the PSO model provided a consistently better empirical description of the experimental data than the PFO model at zeolite dosages of 3.5 and 7.5 g. At 3.5 g, the PSO model yielded an R^2 of 0.9863 compared with 0.9511 for the PFO model, while the SSE decreased from 1.31 to 0.37. At 7.5 g, R^2 increased from 0.9847 to 0.9967 and SSE decreased from 0.09 to 0.02. At 15 g, both models provided an excellent fit ($R^2 \approx 1$), reflecting the very rapid Cu removal and the limited differences between the experimental and calculated profiles.

Table 2. Kinetic parameters obtained from the pseudo-first-order (PFO) and pseudo-second-order (PSO) models for Cu and Pb removal.

Zeolite (g)	Metal	$q_{e,exp}$ (mg g^{-1})	PFO R^2	PFO SSE	k_1 (min^{-1})	$q_{e,PFO}$ (mg g^{-1})	PSO R^2	PSO SSE	k_2 (g mg^{-1} min^{-1})	$q_{e,PSO}$ (mg g^{-1})	Best-Fit Model
3.5	Cu	5.6400	0.9511	1.31	0.2023	5.3620	0.9863	0.367	0.0565	5.6675	PSO

Table 2. *Cont.*

Zeolite (g)	Metal	$q_{e,exp}$ (mg g^{-1})	PFO R^2	PFO SSE	k_1 (min^{-1})	$q_{e,PFO}$ (mg g^{-1})	PSO R^2	PSO SSE	k_2 (g mg^{-1} min^{-1})	$q_{e,PSO}$ (mg g^{-1})	Best-Fit Model
7.5	Cu	2.6320	0.9847	0.09	0.3107	2.5643	0.9967	0.0194	0.2390	2.6491	PSO
15.0	Cu	1.3160	0.9999	1.50×10^{-4}	0.7641	1.3126	1.0000	4.7×10^{-5}	5.7485	1.3166	PSO
3.5	Pb	0.0579	0.9310	2.17×10^{-4}	0.0940	0.0552	0.9715	8.2×10^{-5}	2.7142	0.0589	PSO
7.5	Pb	0.0273	0.9949	3.24×10^{-6}	0.3561	0.0270	0.9988	4.58×10^{-7}	37.6945	0.0274	PSO
15.0	Pb	0.0137	0.99975	4.02×10^{-8}	0.5178	0.0136	0.99985	2.4×10^{-8}	167.8400	0.0137	PSO

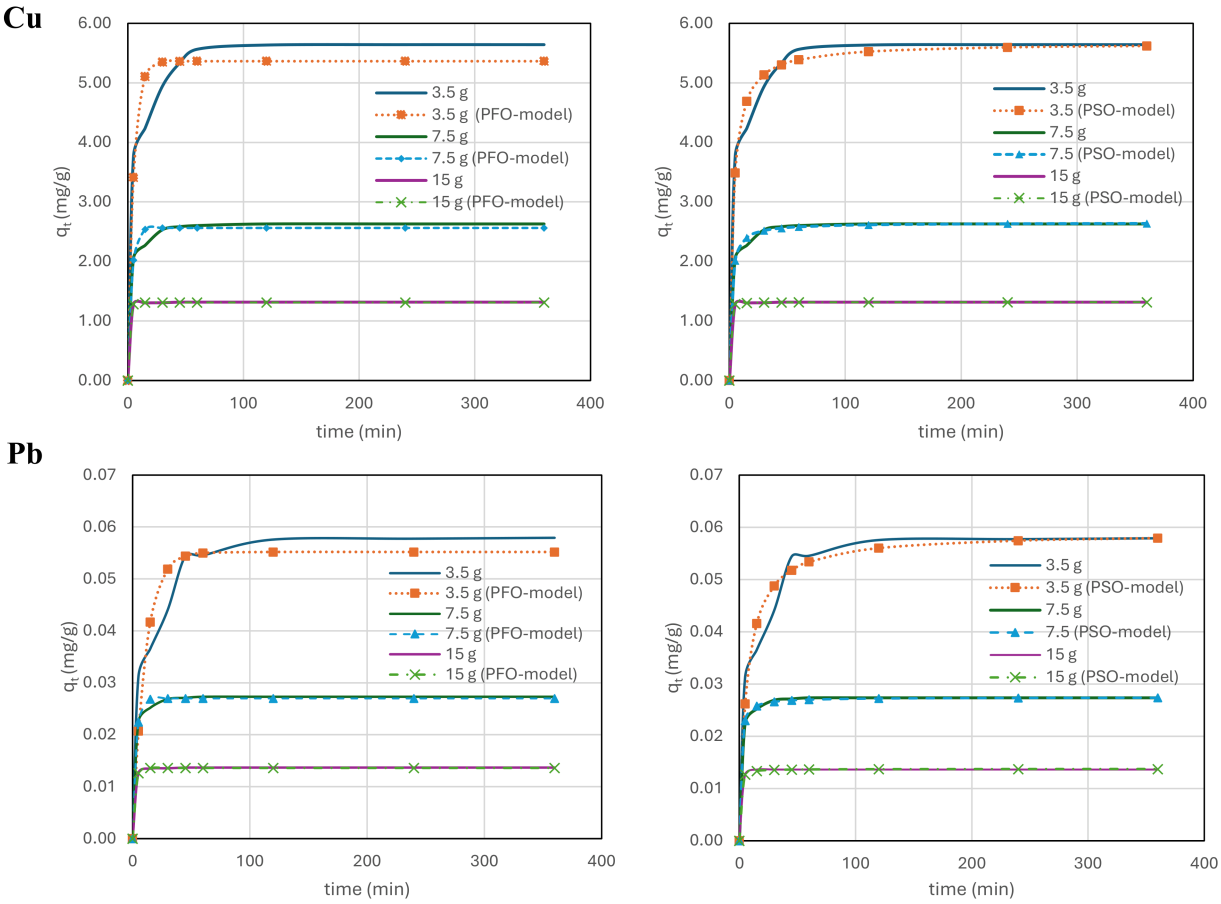


Figure 5. Modeling PFO and PSO of natural zeolite for Cu and Pb.

A similar trend was observed for Pb. The PSO model provided the better empirical fit at 3.5 and 7.5 g, with R^2 values of 0.9715 and 0.9988, respectively, compared with R^2 0.9310 and 0.9949 for the PFO model. At 15 g, both models provided an excellent fit to the experimental data, with R^2 values of 0.99975 for PFO and 0.99985 for PSO. Although the difference was small, the higher R^2 value was obtained with the PSO model; therefore, PSO was retained as the best empirical fit. The apparent convergence of the two models at the highest zeolite dosage should be interpreted cautiously, since the very rapid removal limits the number of experimental points within the main kinetic transition region and therefore reduces the ability to discriminate between the models.

Although the PSO model provided the best statistical fit in most cases, this result should not be interpreted as definitive evidence of chemisorption. In natural zeolite systems, metal removal may involve simultaneous ion exchange, surface interactions, external mass transfer, and diffusion within or around zeolitic particles. Moreover, the present experiments were conducted using real AMD, in which changes in solution chemistry occurred concurrently with metal removal. Therefore, the PSO model is considered here

as an empirical description of the overall kinetic behavior rather than as evidence of a specific molecular mechanism. Similar kinetic behavior has been reported for natural zeolites interacting with metal-bearing aqueous systems, where the observed uptake may involve a combination of ion exchange, surface interactions, and precipitation processes rather than a single controlling mechanism [4,5]. In the present study, this interpretation is particularly relevant because Cu and Pb removal occurred concurrently with a substantial increase in solution pH. Therefore, the kinetic results describe the temporal behavior of aqueous-metal removal, while the specific contributions of sorption, ion exchange, and precipitation cannot be quantitatively separated from the present experiments.

Overall, kinetic modeling indicates that the PSO equation provides the better empirical description of the observed Cu and Pb removal profiles under the experimental conditions investigated. However, the kinetic model alone cannot resolve the mechanisms responsible for Cu and Pb retention. These mechanisms are therefore evaluated together with the pH evolution and the post-treatment mineralogical and microchemical evidence presented in the following sections.

3.3.3. Weber–Morris Intraparticle Diffusion Analysis

Figure 6 shows the Weber–Morris plots used as a complementary assessment of the kinetic behavior of Cu and Pb uptake. Because the experimental curves exhibited non-linear behavior over the complete contact-time range, the Weber–Morris relationship was evaluated over approximately linear regions within the experimental contact-time range rather than by applying a single regression to all experimental points.

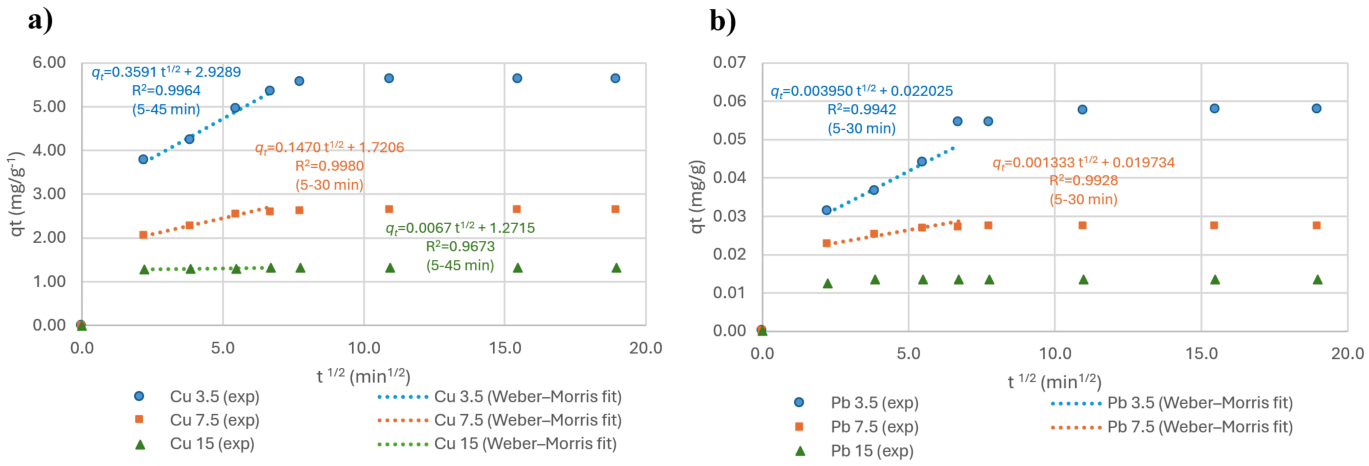


Figure 6. Weber–Morris plots for Cu and Pb removal by natural heulandite–clinoptilolite from real acid mine drainage: (**a**) Cu and (**b**) Pb. Symbols represent experimental q_t values, whereas dashed lines represent linear fits applied only to the experimentally identified approximately linear regions. No Weber–Morris fit was applied to Pb at 15 g because the rapid attainment of the operational plateau did not provide sufficient variation to define a reliable linear region.

For Cu, an approximately linear initial region was identified between 5 and 45 min at 3.5 g of zeolite (k_{id} = 0.3591 mg g^{-1} min$^{-1/2}$, C = 2.9289 mg g^{-1}, R^2 = 0.9964). At 7.5 g, the corresponding region occurred between 5 and 30 min, with k_{id} = 0.1470 mg g^{-1} min$^{-1/2}$, C = 1.7206 mg g^{-1}, and R^2 = 0.9980. At 15 g, Cu uptake approached the operational equilibrium very rapidly, and the identified region between 5 and 45 min showed a substantially lower apparent slope (k_{id} = 0.0067 mg g^{-1} min$^{-1/2}$, R^2 = 0.9673).

For Pb, an approximately linear initial region was identified between 5 and 30 min for both 3.5 and 7.5 g of zeolite, with k_{id} values of 0.00395 and 0.00133 mg g^{-1} min$^{-1/2}$, respectively, and R^2 values of 0.9942 and 0.9928. At 15 g, Pb reached an almost constant q_t

shortly after the initial contact period, providing insufficient variation to define a reliable linear region for Weber–Morris analysis.

The decrease in the apparent slope with increasing zeolite dosage is consistent with the progressively faster approach to the operational equilibrium observed in the removal curves. However, the linear regions identified here are empirical features of the kinetic profiles and cannot be assigned exclusively to a specific mass-transfer mechanism. In particular, the Weber–Morris analysis does not by itself establish intraparticle diffusion as the controlling step. Therefore, these results are interpreted together with the PFO and PSO models and the observed evolution of solution pH.

3.4. Mineralogical and Microchemical Transformation After AMD Treatment

The mineralogical and microchemical observations obtained in this study provide complementary evidence of changes in the recovered zeolitic material following exposure to real AMD. Wingenfelder et al. [4] demonstrated that natural zeolites can remove metal ions from contaminated aqueous systems, while Motsi et al. [5] showed that natural clinoptilolite can remove Cu and Zn from aqueous solutions and emphasized that metal removal may involve processes beyond simple ion exchange. The present results extend this context by integrating real-AMD treatment with time-resolved pH evolution, Cu and Pb removal kinetics, and post-treatment mineralogical and localized microchemical characterization.

In the present system, the persistence of the principal heulandite–clinoptilolite reflections, together with localized Cu-rich regions detected by SEM-EDS and reflections compatible with Cu-exchanged clinoptilolite and Ca–SO_4-bearing phases, indicates that the treatment produced measurable mineralogical and microchemical changes while the principal zeolitic phases remained identifiable. These observations provide complementary evidence for metal association with the recovered solid, although they do not allow the relative contribution of ion exchange, surface association, and precipitation to be quantified.

3.4.1. X-Ray Diffraction Analysis

The mineralogical changes in the natural zeolite before and after AMD treatment were evaluated by X-ray diffraction (XRD). Figure 7 shows the XRD patterns of the untreated zeolite (a), the post-treatment material (b), and an enlarged view of the selected diffraction region (c). The untreated material was predominantly identified as Ca-bearing heulandite and Ca-bearing clinoptilolite, confirming the heulandite–clinoptilolite nature of the starting material. The persistence of the main zeolitic reflections after treatment is consistent with previous observations of natural zeolites used for metal removal from mine waters [4].

After AMD treatment, the main heulandite reflections remained identifiable, indicating that the principal zeolitic crystalline phases persisted under the experimental conditions. However, the XRD results do not quantify the extent of structural alteration. The post-treatment pattern also showed correspondence with a Cu-exchanged clinoptilolite reference phase. Considering the near-complete removal of Cu from the aqueous phase and the localized Cu-rich regions detected by SEM-EDS, this result supports a Cu-associated chemical modification of the clinoptilolitic component. However, the XRD data alone do not demonstrate that Cu incorporation occurred exclusively through ion exchange. Additional reflections compatible with anhydrite and bassanite were identified in the post-treatment material. Given the high sulfate concentration of the AMD, these matches are consistent with the possible presence of Ca–SO_4-bearing secondary phases. Nevertheless, their formation during treatment cannot be conclusively established from phase matching alone. Because the AMD solution was not subjected to post-treatment sulfate and calcium speciation analyses, the origin and extent of any Ca–SO_4-bearing phase formation cannot be quantitatively established from the present data. Other minor phases identified by the

matching procedure, including albite, quartz, and srebrodolskite, were not considered sufficient evidence of treatment-induced mineral formation. Overall, the XRD results indicate that AMD treatment produced detectable changes in the mineralogical signature of the zeolite, particularly in the clinoptilolitic component, while the principal zeolitic crystalline phases remained identifiable after treatment.

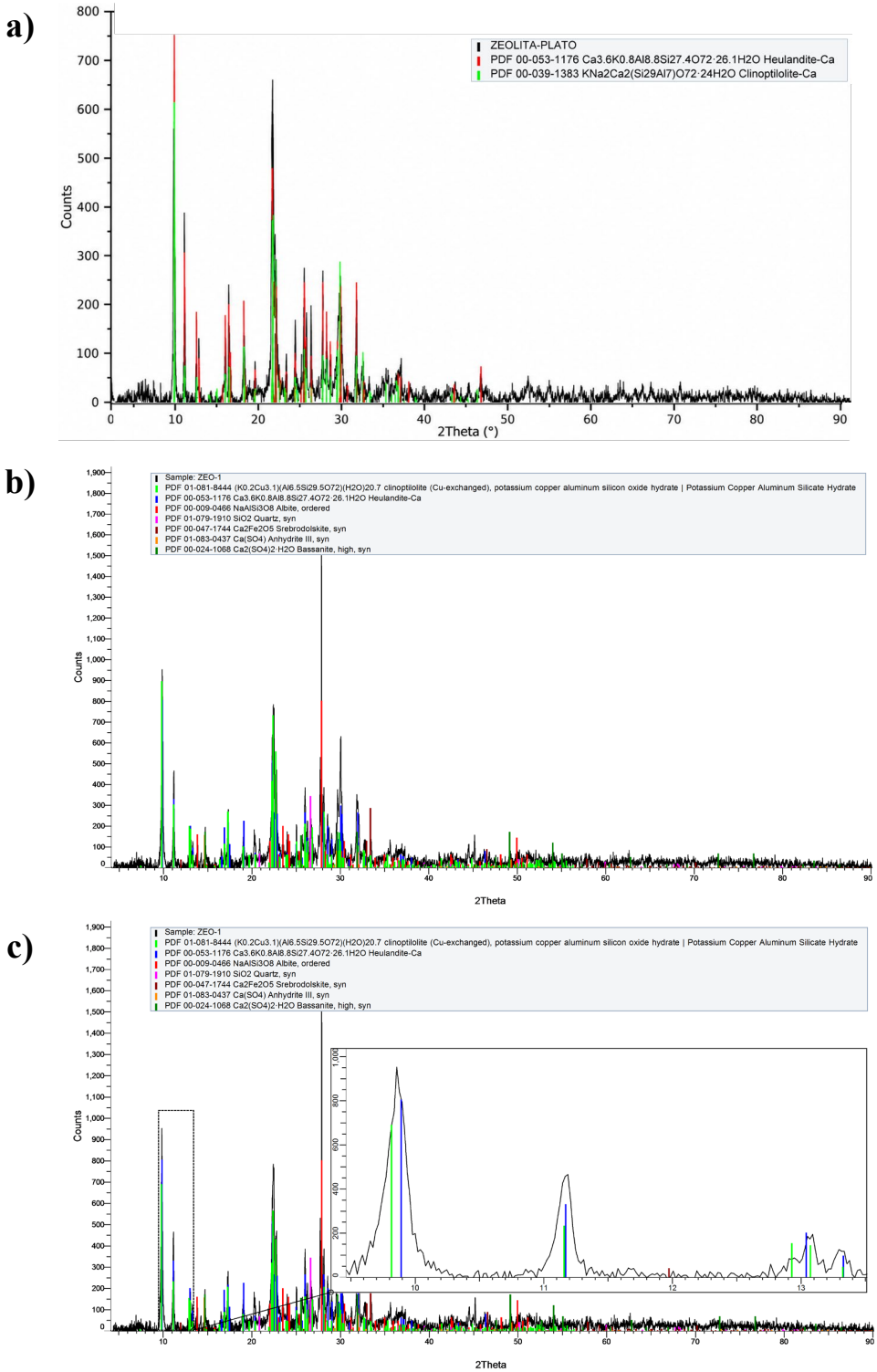


Figure 7. XRD patterns of the natural zeolite before and after AMD treatment: (**a**) untreated zeolite, (**b**) post-treatment zeolite, and (**c**) enlarged view of the selected diffraction region showing the main zeolitic phases and mineralogical changes after treatment.

3.4.2. Localized Microchemical Transformations Revealed by SEM-EDS

SEM-EDS analysis provided evidence of localized chemical changes in the zeolite after AMD treatment (Figure 8). The untreated material exhibited an aluminosilicate composition dominated by O, Si, and Al, with Na and K as minor constituents, whereas Cu and S were not detected in the analyzed region. After treatment, distinct Cu-rich regions were identified, with Cu concentrations of 28.85, 52.09, and 34.91 wt.% in three representative analyses. These regions also contained Si, Al, and O, with variable contributions of Na and Ca.

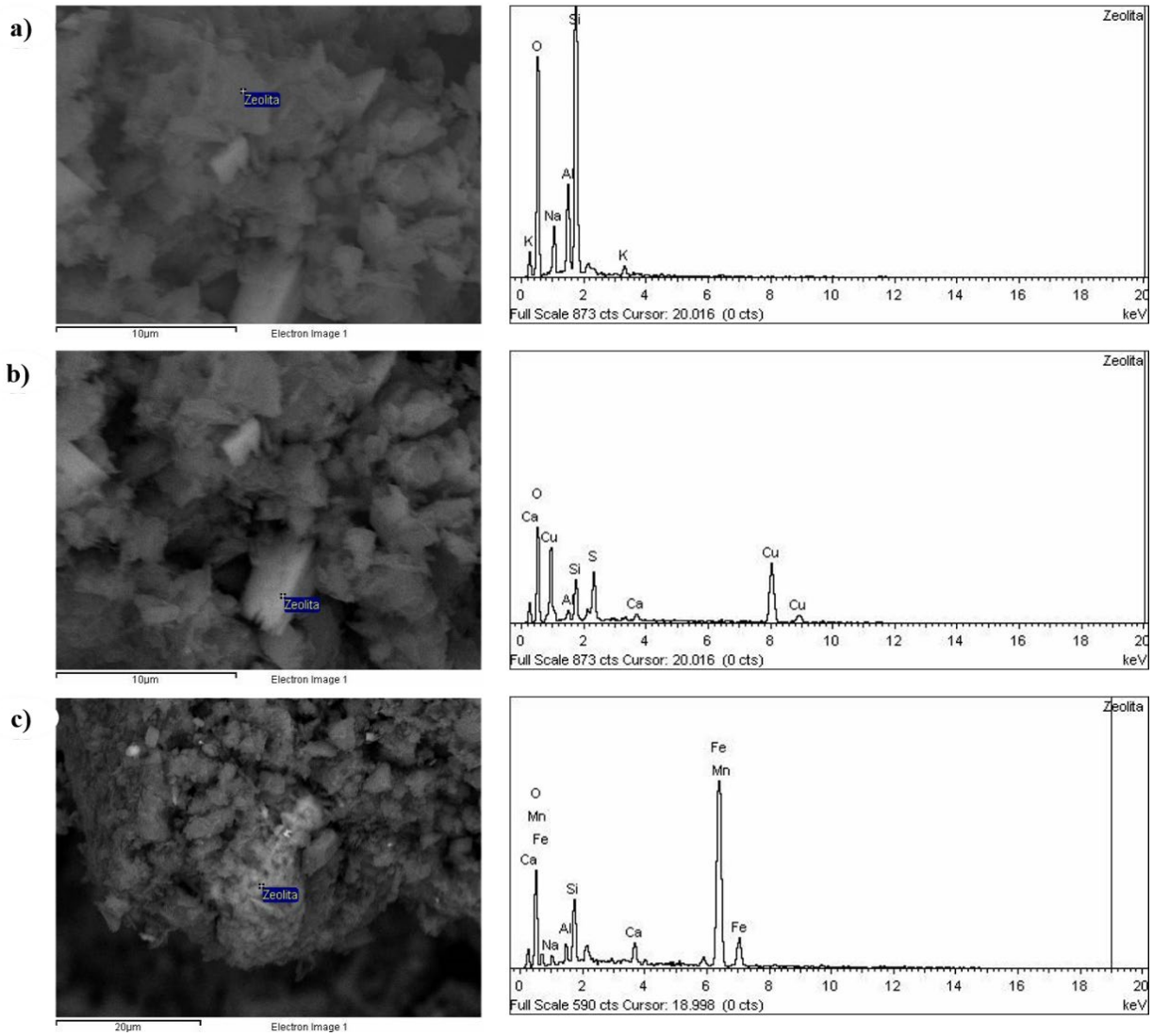


Figure 8. SEM-EDS characterization of the natural heulandite–clinoptilolite zeolite before and after AMD treatment: (**a**) untreated zeolite and corresponding EDS spectrum; (**b**) post-treatment zeolite showing a Cu-rich region and corresponding EDS spectrum; and (**c**) post-treatment zeolite showing an Fe-rich region and corresponding EDS spectrum.

The occurrence of localized Cu-rich regions, together with the correspondence of the post-treatment XRD pattern with a Cu-exchanged clinoptilolite reference phase and the near-complete removal of Cu from the AMD, provides converging evidence for Cu association with the zeolitic material. The lower relative Na content observed in some Cu-rich regions is qualitatively consistent with cation exchange; however, because SEM-EDS measurements are highly localized and no bulk elemental balance was performed for the

solid phase, the relative contributions of ion exchange, surface association, and possible precipitation cannot be quantitatively distinguished.

In contrast, Pb was not detected in the analyzed SEM-EDS regions or in the post-treatment XRD pattern, despite its near-complete removal from the aqueous phase. Given the relatively low initial Pb concentration in the AMD (2.05 mg L^{-1}), the absence of a Pb signal by localized SEM-EDS does not demonstrate the absence of Pb from the recovered zeolite. Rather, it indicates that Pb was below the effective detection capability of the localized characterization under the analytical conditions employed, or that it was present in a highly dispersed, amorphous, or otherwise undetectable form. Consequently, the final solid-phase distribution of Pb cannot be established from the available SEM-EDS and XRD data. A bulk chemical digestion of the recovered zeolite followed by ICP-based analysis, preferably ICP-MS for low-level Pb determination, would be required to quantitatively assess the amount of Pb associated with the solid and to establish a solid-phase Pb balance.

Localized Fe-rich regions were also identified after treatment, reaching 65.09 and 33.63 wt.% Fe in representative point analyses. No Fe was detected in the representative untreated zeolite analyzed by SEM-EDS. Therefore, the appearance of Fe-rich regions after exposure to AMD indicates that Fe became locally associated with the zeolitic material during treatment. The initial AMD contained 0.19 mg L^{-1} Fe, slightly above the analytical LOQ of 0.1656 mg L^{-1}. Because SEM-EDS provides localized rather than bulk compositional information, the high Fe contents measured in selected regions cannot be interpreted as representative of the overall Fe content of the recovered zeolite or as a quantitative measure of Fe uptake. The observed Fe association may involve surface retention, ion exchange, precipitation, or a combination of these processes, particularly in view of the simultaneous increase in solution pH. The present results demonstrate localized Fe association with the treated zeolite, but do not allow the specific retention mechanism or total amount of Fe retained by the solid to be quantitatively established.

Overall, SEM-EDS demonstrates that AMD treatment produced pronounced but spatially localized chemical modifications, particularly Cu enrichment, while the main zeolitic phases remained identifiable by XRD. The contrasting solid-phase signatures observed for Cu, Pb, and Fe highlight that removal from the aqueous phase does not necessarily result in an equivalent or detectable solid-phase signature.

3.5. Integrated Interpretation of Zeolite–AMD Interaction

The combined aqueous-phase, kinetic, and solid-phase results indicate that the interaction between natural heulandite–clinoptilolite and real AMD involves simultaneous changes in solution chemistry and localized modification of the zeolitic material. The initial AMD had a pH of 3.6, which increased rapidly after contact with the zeolite and reached final values of 4.30, 5.20, and 6.20 at zeolite dosages of 3.5, 7.5, and 15.0 g per 100 mL, respectively. Most of this change occurred during the first 30–60 min, coinciding with the period of rapid Cu and Pb removal. The dose-dependent response indicates that the zeolite substantially altered the acid–base conditions of the AMD during treatment. Such behavior is consistent with the ion-exchange and acid–base reactivity reported for natural zeolites and with the pH response observed during clinoptilolite treatment of natural AMD [3,8]. The segmented Weber–Morris analysis further indicates that the uptake curves are not adequately represented by a single linear relationship over the complete contact-time range. The apparent decrease in slope with increasing zeolite dosage is consistent with the faster approach to operational equilibrium at higher solid loading. However, these empirical kinetic regions do not provide sufficient evidence to assign a single controlling mass-transfer mechanism.

The Cu results provide the strongest evidence for a detectable solid-phase transformation. Nearly complete Cu removal from the aqueous phase was accompanied by the appearance of localized Cu-rich regions in SEM-EDS and by XRD reflections compatible with a Cu-exchanged clinoptilolite reference phase. The convergence of these observations supports a Cu-associated modification of the clinoptilolitic component of the zeolite. However, the localized nature of the SEM-EDS measurements prevents their use as a bulk chemical balance, and the available evidence does not allow the relative contributions of ion exchange, surface association, and possible precipitation to be quantified. Therefore, Cu retention is better interpreted as the result of coupled chemical interactions rather than as evidence for a single isolated mechanism.

The behavior of Pb was markedly different. Although Pb was almost completely removed from the aqueous phase, no Pb-bearing phase was identified by XRD and Pb was not detected in the analyzed SEM-EDS regions. This contrast demonstrates that aqueous removal cannot necessarily be equated with the formation of a detectable crystalline or locally enriched solid phase. Pb may have been retained in a highly dispersed, amorphous, or otherwise undetectable form, but its final solid-phase association cannot be established from the present characterization.

Overall, the results indicate that real AMD treatment induced chemical and microchemical modification of the natural zeolite while the principal zeolitic crystalline phases remained identifiable after treatment. The observed increase in pH, rapid metal removal, Cu-rich domains, possible Ca–SO_4-bearing secondary phases, and localized Fe-rich regions collectively indicate that zeolite–AMD interaction is more complex than a simple adsorption process. The appearance of Fe-rich regions after treatment, together with the absence of detectable Fe in the representative untreated zeolite, is consistent with localized Fe association with the recovered material. However, the present SEM-EDS results do not allow the total amount of Fe retained or the specific Fe-bearing phase and retention mechanism to be established. Importantly, the main heulandite–clinoptilolite phases remained identifiable after treatment, although the extent of structural alteration cannot be quantitatively determined from the present XRD data. This distinction between persistence of the principal crystalline phases and localized chemical modification provides a basis for future investigations of regeneration and reuse of natural zeolite for AMD treatment.

Previous studies have demonstrated the effectiveness of natural zeolites for removing dissolved metals from mine waters and AMD [5–8]. The present results extend this understanding by showing that metal removal occurs concurrently with measurable changes in solution pH and localized chemical modification of the zeolitic material, while the principal crystalline phases remain identifiable after treatment.

Compared with previous studies of natural zeolites for metal removal, the present work provides an integrated evaluation of zeolite interaction with real AMD rather than a simplified single-metal or synthetic aqueous system. The study combines the evolution of solution pH, Cu and Pb removal kinetics, empirical kinetic modeling, and post-treatment XRD and SEM-EDS characterization within the same experimental framework. This integrated approach shows that natural Ca-bearing heulandite–clinoptilolite can substantially modify the aqueous chemistry of real AMD while simultaneously accumulating Cu and producing detectable mineralogical and localized microchemical changes in the recovered solid. The results therefore contribute to a more comprehensive understanding of the coupled aqueous–solid response of natural zeolite during AMD treatment while also highlighting the limitation that removal cannot be attributed exclusively to sorption without dedicated precipitation controls.

4. Conclusions

Under the investigated batch conditions, natural heulandite–clinoptilolite achieved near-complete removal of dissolved Cu and Pb from real acid mine drainage. Increasing the zeolite dosage accelerated metal removal and reduced the contact time required to achieve near-complete removal, although the metal uptake per unit mass decreased as the zeolite dosage increased.

The interaction with AMD produced a rapid and dose-dependent increase in pH, from an initial value of 3.6 to 4.3, 5.2, and 6.2 with 3.5, 7.5, and 15.0 g of zeolite, respectively. Most of the pH change occurred during the first 30–60 min, coinciding with the period of rapid Cu and Pb removal. This temporal association indicates that metal uptake occurred concurrently with substantial changes in solution chemistry, although the present data do not allow the individual contributions of acid–base reactions, ion exchange, and other processes to be quantified.

Post-treatment characterization demonstrated that the principal zeolitic crystalline phases remained identifiable after AMD treatment. The post-treatment XRD pattern showed reflections compatible with Cu-exchanged clinoptilolite, while SEM-EDS revealed localized Cu-rich regions containing up to 52.09 wt.% Cu. Together with near-complete aqueous Cu removal, these observations provide converging evidence for Cu association with the zeolitic material, although the relative contributions of ion exchange, surface association, and possible secondary-phase formation cannot be quantitatively resolved.

In contrast, Pb was efficiently removed from the aqueous phase but was not detected in the analyzed post-treatment XRD or SEM-EDS results. Therefore, its final solid-phase form and retention mechanism remain unresolved. Localized Fe-rich regions were also observed after treatment, whereas no Fe was detected in the representative untreated zeolite. Their occurrence is therefore consistent with localized Fe association with the zeolitic material during AMD treatment. However, because the initial Fe concentration was only slightly above the analytical LOQ (0.1656 mg L^{-1}) and SEM-EDS provides localized rather than bulk compositional information, the total amount of Fe retained and the specific Fe-bearing phase or retention mechanism cannot be quantitatively established.

Overall, the results demonstrate that treatment of real AMD with natural heulandite–clinoptilolite involves chemical and microchemical modification while the principal zeolitic crystalline phases remained identifiable after treatment. The contrasting behavior of Cu, Pb, and Fe highlights the complexity of Cu and Pb retention in real AMD and demonstrates that aqueous removal does not necessarily result in an equivalent detectable solid-phase signature. Further studies using real AMD should focus on elemental mass balances, metal speciation, and regeneration–reuse cycles to clarify metal immobilization mechanisms and evaluate the long-term applicability of the zeolite.

Author Contributions: G.A.-M.: Data curation, Methodology; D.P.N.-G.: Methodology, Data curation; J.A.-M.: Formal analysis; E.E.-S.: Formal analysis, Writing-review; I.A.R.: Methodology, Data curation; G.R.-M.: Investigation; Conceptualization; Methodology; Formal analysis, Writing—review & editing, Data curation. All authors have read and agreed to the published version of the manuscript.

Funding: This research received no external funding.

Data Availability Statement: The data supporting the findings of this study are available from the corresponding authors upon reasonable request.

Acknowledgments: The authors gratefully acknowledge the management support of Manuel Martínez, Rosalina Tovar, and Francisco Galindo, for their contributions to project management.

Conflicts of Interest: The authors declare no conflict of interest.

References

1. Johnson, D.B.; Hallberg, K.B. Acid mine drainage remediation options: A review. *Sci. Total Environ.* **2005**, *338*, 3–14. [CrossRef]
2. Akcil, A.; Koldas, S. Acid mine drainage (AMD): Causes, treatment and case studies. *J. Clean. Prod.* **2006**, *14*, 1139–1145. [CrossRef]
3. Wang, S.; Peng, Y. Natural zeolites as effective adsorbents in water and wastewater treatment. *Chem. Eng. J.* **2010**, *156*, 11–24. [CrossRef]
4. Wingenfelder, U.; Hansen, C.; Furrer, G.; Schulin, R. Removal of heavy metals from mine waters by natural zeolites. *Environ. Sci. Technol.* **2005**, *39*, 4606–4613. [CrossRef]
5. Motsi, T.; Rowson, N.A.; Simmons, M. Adsorption of heavy metals from acid mine drainage by natural zeolite. *Int. J. Miner. Process.* **2009**, *92*, 42–48. [CrossRef]
6. Varvara, S.; Popa, M.; Bostan, R.; Damian, G. Preliminary considerations on the sorption of heavy metals from acidic mine drainage using natural zeolite. *J. Environ. Prot. Ecol.* **2013**, *14*, 1506–1514.
7. Markovic, R.; Gardic, V.; Obradovic, L.; Djordjievski, S.; Stevanovic, Z.; Stevanovic, J.; Gvozdenovic, M. The application of a natural zeolite for acid mine drainage purification. *Mater. Trans.* **2015**, *56*, 2053–2057. [CrossRef]
8. Ekolu, S.O.; Ramoetlo, N.; Solomon, F. Clinoptilolite zeolite use as adsorbent for removal of metal contaminants from natural acid mine drainage. *Water Sci.* **2026**, *40*, 8. [CrossRef]
9. Lagergren, S. Zur Theorie der sogenannten Adsorption gelöster Stoffe. In *Kungliga Svenska Vetenskapsakademiens Handlingar*; Royal Swedish Academy of Sciences: Stockholm, Sweden, 1898; Volume 24, pp. 1–39.
10. Ho, Y.S.; McKay, G. Pseudo-second order model for sorption processes. *Process Biochem.* **1999**, *34*, 451–465. [CrossRef]
11. Weber, W.J., Jr.; Morris, J.C. Kinetics of adsorption on carbon from solution. *J. Sanit. Eng. Div.* **1963**, *89*, 31–59. [CrossRef]

Disclaimer/Publisher's Note: The statements, opinions and data contained in all publications are solely those of the individual author(s) and contributor(s) and not of MDPI and/or the editor(s). MDPI and/or the editor(s) disclaim responsibility for any injury to people or property resulting from any ideas, methods, instructions or products referred to in the content.